Computers and Geotechnics 70 (2015) 150–158

Contents lists available at ScienceDirect

Computers and Geotechnics

journal homepage: www.elsevier.com/locate/compgeo

Research Paper

Simulating flows in multi-layered and spatially-variable permeability media via a new Gray Lattice Boltzmann model

A. Yehya [a,b,*], H. Naji [a,b], M.C. Sukop [c]

[a] Civil Engineering and Geo-Environment Laboratory, Artois University, 62400 Béthune, France
[b] Lille University, Northern France, 59000 Lille, France
[c] Department of Earth and Environment, Florida International University, Miami, FL 33199, USA

ARTICLE INFO

Article history:
Received 6 May 2015
Received in revised form 29 July 2015
Accepted 31 July 2015

Keywords:
Lattice Boltzmann model
Porous medium
Porosity
Permeability
Darcy's flow

ABSTRACT

The simulation of flow in porous and fibrous permeable media is of high importance in many scientific and industrial applications. Although the finite element models at the representative elementary volume scales are used to solve a huge amount of scientific and engineering problems, they are hardly used to efficiently simulate pore-fluid flow problems at the particle scales. This encourages the development of numerical models to match the needs of such studies. In this paper, we propose a new Gray Lattice Boltzmann numerical model for simulating fluid flow in permeable media. Unlike most previous models, our proposed model has the ability to simulate multi-layers and space-variable permeability while preserving the continuity of the macroscopic velocity field. The model is verified with the available analytical solutions and a derived analytical expression for the case of variable porosity. In addition, we examine the importance of introducing a transition layer with a defined porosity function near the boundaries and interfaces. If this layer exists in practice, then the numerical results reveal that it cannot be neglected, and its impact is significant on the obtained velocity distribution. Finally, in the light of the obtained results, we can state that the proposed model has great potential to simulate complex and heterogeneous media with smoothness and accuracy, so that it may enrich the research content of the emerging computational geosciences.

1. Introduction

Many natural substances, such as rock and soil, and manufactured materials, such as cements and ceramics, can be considered as porous media. The concept of porous media is used in many areas of applied science, materials science, and engineering. Their applications can be found in various fields of research such as geo-sciences [1,2], environmental studies [3–5], hydrology [6,7], subsurface flows [8,9], hydrocarbon recovery [10,11], and so forth. Therefore, understanding and simulating fluid flow through complex porous media is a common interest. However, computing the permeability is a challenging task since this parameter depends entirely on the extremely heterogeneous and complex microstructure [12]. So, to numerically model a porous material, we should either have detailed information on the structure (which enables explicit flow simulation at a micro-scale pore/solid level) or at least an estimated porosity of a representative elementary volume [13–15] (see Fig. 1). If a representative elementary volume (REV) can be determined, we typically assume that any larger volume of the same medium will have approximately the same averaged properties, such as porosity, permeability and anisotropy.

Note that to understand the dynamic mechanisms of crustal ore-forming systems, Zhao and his coworkers have conducted systematic and pioneering studies [1–3] on the numerical simulation of porous fluid flow problems associated with mineral forming processes, resulting in the establishment of the emerging computational geosciences field. Since a mineral deposit is the direct consequence of a fully-coupled problem between rock deformation, fluid flow, heat transfer, reactive mass transport processes, it is inevitable to establish some numerical methods to simulate porous fluid flow associated with ore body formation and mineralization within the Earth's crust [16–18]. Thus, the finite element (FE) models at the REV scales have been successfully established to simulate: (1) pore-fluid flow induced chemical dissolution problems in subsurface systems [19–22]; (2) pore-fluid convective flow within large-scale geological systems [23–25]; (3) pore-fluid flow induced contaminant transport problems in geo-environmental systems [26–28]; and (4) non-isothermal fluid flow problems in

* Corresponding author at: Civil Engineering and Geo-Environment Laboratory, Artois University, 62400 Béthune, France.
E-mail address: alissar.yehya@gmail.com (A. Yehya).

http://dx.doi.org/10.1016/j.compgeo.2015.07.017
0266-352X/

Nomenclature

Lattice	(Units)
lu	Lattice unit of length
ts	Lattice unit of time
mu	Lattice unit of mass

Symbols

c_s	sound of speed (lu/ts)
e_i	Lattice velocity in direction i (lu/ts)
f	density distribution function (–)
L_x	channel length (lu)
L_y	channel width (lu)
p	pressure (mu/lu^2)
q	flow rate (lu^3/ts)
U_n	normalized velocity (lu/ts)
u	macroscopic velocity (lu/ts)
k	permeability (lu^2)
x_s	scatter density (–)
w	transition layer width (lu)

Greek symbols

ω	weight factor (–)
ρ	macroscopic density (mu/lu^3)
ϕ	solid fraction (–)
ν	kinematic viscosity (lu^2/ts)
τ_f	relaxation parameter (–)

Subscripts/superscripts

col	collision
eq	equilibrium
i	Lattice direction
in	In
out	Out
x	along x-direction
y	along y-direction

fluid-saturated rocks [29,30]. Although the FE models at the REV scales are used to solve a huge amount of scientific and engineering problems [16–30], they are hardly used to efficiently simulate pore-fluid flow problems at the particle scales [31]. For this reason, several particle-based methods, one of which is the LBM, have been developed to enrich the research contents of the emerging computational geosciences.

Many porous media are variable and heterogeneous at particular scales of interest, hence in our paper, to easily handle complex porous media with variable permeability, we use the "Gray" mesoscopic particle-based Lattice Boltzmann method (GLBM). This method can simultaneously simulate porous media at the pore/solid scale and at scales where the porous medium is represented as a permeability field. However, to simulate heat transfer and reactive mass transport in porous media using the GLBM, there remains much to be done in the future.

Interest for LBMs has been growing continuously in the last 20 years [32,33]. LBMs have been successfully applied to simulate laminar, turbulent, and multiphase fluid flows, heat and mass transport, and also flow in porous media [32–35]. This approach was developed following the pioneering works of Rothman [36] on LGCA and Succi et al. [37] on the Lattice Boltzmann Equation (LBE). Unlike traditional numerical methods, which solve for the macroscopic variables, the LBM is based on the kinetic equation for the particle distribution function. Hence, the macroscopic quantities are obtained through moment integration of the density distribution function, and the averaged fluid variables are shown to satisfy the Navier–Stokes equations (NSEs) [38]. The local nature of this method, wherein complex wall boundaries can be easily incorporated, encourages its use in the simulation of flow in porous media and complex structures.

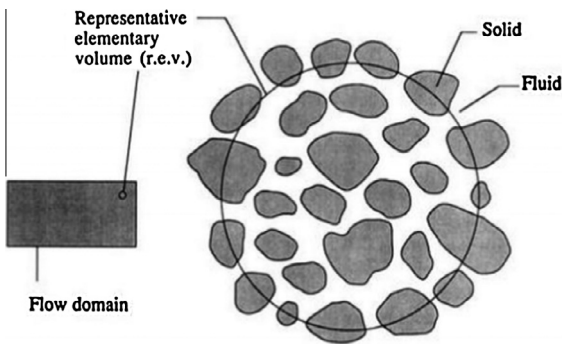

Fig. 1. Representative elementary volume (REV) of a porous medium.

The implementation of a porous medium model using LBM is usually attained by the definition of a parameter that defines the state of a lattice. This parameter defines the solid fraction at a lattice node and differentiates between fluid, solid, and porous solid nodes. The key here is to correctly model the resistance of porous solids to fluid flow [39]. To do this, two approaches of fluid flow are proposed in the literature. The first introduces a resistance force to mimic the behavior of fluid flow through porous or fibrous media. This resistance force functions as to render the velocity field to zero for the solid nodes, to follow the Darcy-Brinkman equations in porous zones, and to recover the Navier–Stokes equations in the case of fully fluid nodes. Extensive description of this approach can be found in [40–43]. According to Zhu et al. [39], despite the fact that this approach has been applied for modeling fluid flow at a regional scale [44], the Chapman-Enskog expansion for deriving the corresponding macroscopic equations may break down [45,46]. On the other hand, the second approach applies the partial bounce-back rule on the lattice nodes of certain permeability value to mimic the needed resistance, and hence fully blocks the velocity field in the case of solid nodes or adopts the normal Navier–Stokes regime for fully fluid nodes. Most LBMs that use this approach are called Gray Lattice Boltzmann (GLB) models [39]. For more details on this procedure, one can refer to the works of McCloskey et al. [47,48], Sukop et al. [32,49], and Walsh et al. [50]. The difference between these works is in the implementation of the bounce-back rule, where the first proposed an outgoing bounce-back, the second employed it as pre-collision step, while the third used a post-collision procedure. Unlike the first two models, the partial bounce-back approach used by Walsh et al. [50] conserves mass in heterogeneous media and shows improvements in simulating buoyancy-driven flow as well as diffusive processes. Nevertheless, as reported in [39], the model of Walsh et al. [50] shows discontinuity at interfaces in the velocity when used for multiple layers of different permeability values. Thus, in this paper, we adopt a single-relaxation Lattice Boltzmann model with a partial-bounce back approach to mimic the porous medium, but our model will sufficiently insure the continuity at layer interfaces. This proposed

model defines global parameters that insure any user-defined data, on the nodes, including the permeability, porosity, or viscosity. Note that the performance of the model against these variable parameters, and its ability to capture Darcy-Brinkman flow at interfaces, will be verified by deriving analytical solutions for the studied cases.

The paper is organized as follows. In the second section, the concept description and numerical model are presented. The applied LBM is briefly described along with the implementation of the porous medium model. A descriptive comparison with previous models is provided and the major enhancements are discussed. In the third section, an expression to relate the solid fraction global model parameter to the actual scatter density is obtained. The model is then checked with respect to the analytical solutions of the proposed problem and for different patterns. Later in the fourth section, the continuity of the velocity field at interfaces is discussed and the model's ability to simulate multi-layer flow problems is successfully demonstrated. The next section is dedicated to setting the solid fraction parameter as a variable in space. The model is then verified with a derived analytical solution for both constant and spatially-variable permeability. The last section is an application defining a space-dependent porosity and its importance for practical purposes. Variable permeability transition layers are constructed near solid walls and their influence on the macroscopic parameters is examined. Finally, major conclusions are presented while highlighting some comments on the main results.

2. Model description

The LBM [32–35,37,38] consists of simulating the statistical behavior of a set of particles on a lattice with finite velocities. It stems from the discrete Boltzmann equation and allows determination of macroscopic fluid properties such as density, velocity and pressure through weighted averages, or moments, of the particle distribution for all discrete lattice velocities. The spatial discretization and the time step define the units of the simulations. The density distribution is determined through two steps, which are collision and streaming (advection) processes, and has the form given in Eq. (1):

$$\begin{aligned} f_i\left(\vec{x}+\Delta x, t+\Delta t\right) &= f_i\left(\vec{x}, t\right) - \tau_f^{-1}\left(f_i(\vec{x}, t) - f_i^{eq}(\vec{x}, t)\right) \\ f_i\left(\vec{x}+\vec{e}_i, t+1\right) &= f_i\left(\vec{x}, t\right) - \tau_f^{-1}(f_i(\vec{x}, t) - f_i^{eq}(\vec{x}, t)) \end{aligned} \quad (1)$$

where $\vec{e}_i$ is the microscopic particle velocity in the i-direction and τ_f is the dimensionless relaxation time. Recall that, we use here the units for the lattice grid spacing and the time step of $(\Delta x = \Delta t = 1)$ such that all the relevant quantities are dimensionless. f_i^{eq} is the local equilibrium distribution function that has the following form for the D2Q9 model:

$$f_i^{eq} = \rho\omega_i\left[1 + \frac{3(\vec{e}_i.\vec{u})}{c_s^2} + \frac{9(\vec{e}_i.\vec{u})^2}{2c_s^4} - \frac{3(\vec{u}.\vec{u})}{2c_s^2}\right] \quad (2)$$

$$\text{where} \quad \omega_i = \begin{cases} 4/9 & \text{for} \quad i = 0 \\ 1/9 & \text{for} \quad i = 2,4,6,8 \\ 1/36 & \text{for} \quad i = 0,3,5,9 \end{cases} \quad \text{and}$$

$$\vec{e}_i = \begin{cases} (0,0) & \text{for} \quad i = 0 \\ (0,\pm 1) & \text{for} \quad i = 2,4 \\ (\pm 1,0) & \text{for} \quad i = 1,3 \\ (\pm 1,\pm 1) & \text{for} \quad i = 5,6,7,8 \end{cases} \quad (3)$$

are, respectively, the weight coefficient and the velocity vector of the D2Q9 model; $\vec{u}(u_x, u_y)$ is the macroscopic velocity, with u_x and u_y representing velocities in the x- and y-direction, respectively. Note that the relaxation time τ_f can be determined via $\nu = c_s^2\Delta t(\tau_f - 0.5)$, c_s being the lattice sound speed (1/3 for the D2Q9 model), and ν being the kinematic viscosity.

The basic hydrodynamic properties, such as density, ρ, and momentum density, ρu, are defined as moments of the distribution function (DF), f_i, as follows,

$$\rho = \sum_{i=0}^{n=8} f_i \quad \text{and} \quad \rho\vec{u} = \sum_{i=0}^{n=8} \vec{e}_i f_i \quad (4)$$

As stated above, Eq. (1) is usually solved in two steps, i.e. streaming and collision.

$$f_i^*(\vec{x}, t) - f_i(\vec{x}, t) = \tau_f^{-1}(f_i(\vec{x}, t) - f_i^{eq}(\vec{x}, t)) \quad (5)$$

$$f_i^*(\vec{x} + \vec{e}, t+1) = f_i^*(\vec{x}, t) \quad (6)$$

Detailed introductions to LBMs can be found in Sukop and Thorne [32], Succi [34], to name a few.

However, to simulate the porous medium in our model, we will introduce a solid fraction parameter, ϕ, to define the effective porosity $(1-\phi)$ that determines the permeability of the medium. It actually describes the percentage of solids to be subjected to bounce-back at a lattice node within the model. Hence, as suggested by Walsh et al. [50], we add a step to redirect the incoming fluid packets prior to the collision step (Eq. (7)). However, as an enhancement to the previous model, our model insures the continuity in the velocity field even if the parameter ϕ is variable in space.

$$f_i^{out}(\vec{x}, t) = (1-\phi)f_i^{col}(\vec{x}, t) + \phi f_i^{in}(\vec{x}, t) \quad (7)$$

Note that the model behaves as follows: The full bounce-back is recovered when $\phi = 1$, while for $\phi = 0$, a normal fluid node is assigned and hence normal collision is conducted. Using this method, the mass conservation is respected as demonstrated by the previous work [50].

Moreover, the average velocity, in the presence of ϕ will be expressed in terms of the incoming fluid packet densities as

$$\vec{u}' = \frac{1-\phi}{\rho}\sum_i \vec{e}_i f_i^{in} \quad (8)$$

This definition of the average velocity with the partial bounce-back scheme insures setting the whole field to zero when fully solid $(\phi = 1)$, or returning to the Navier–Stokes regime when we have full fluid $(\phi = 0)$. When we have $(0 \leqslant \phi \leqslant 1)$, the Darcy–Brinkman flow for permeable media is captured.

Furthermore, the introduced solid fraction parameter, ϕ, will insure that any user-defined data concerning the permeability, or porosity of each node in the system are honored. This flexibility allows the possibility to define a realistic heterogeneous porous medium, if we have the necessary data, or to evaluate an effective permeability to describe a layer or zone in the modeled system.

3. Model's verification

To validate our model, we compare the numerical results to the analytical solution of the Darcy–Brinkman equation for the problem illustrated in Fig. 2. The parameters summarized in Table 1 indicate the different simulation cases used throughout the verifications.

It is useful to note that the solid fraction, ϕ, should be regarded as an internal model parameter from which the permeability is derived, rather than a reflection of the actual proportion of solid material at each node [23]. Hence, we established a relation

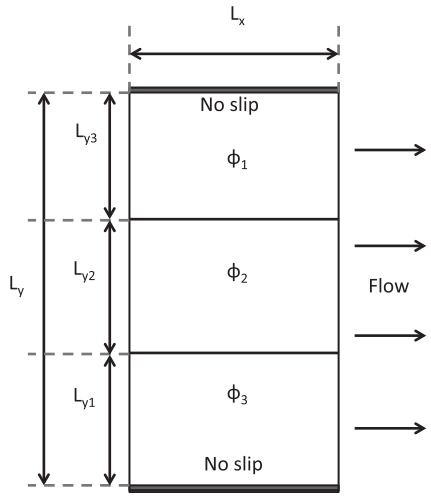

Fig. 2. Schematic view of the studied multi-layer flow.

(Eq. (9)) between our model's parameter, ϕ, and the number of scatters, x_s, to satisfy the Darcy–Brinkman equation.

$$\phi = 1 - \left(\frac{1.2865}{1 + e^{(x_s - 0.1)/0.08}}\right) \tag{9}$$

This relationship assures that when the scatter density, x_s, tends to 0 or 1, the parameter, ϕ, will also tend respectively to 0 or 1. In addition, this will insure that the velocity field will be almost blocked for $\phi \geqslant 0.5$. However, in the present model, when $\phi = 0$, the Navier–stokes flow is recovered and the permeability tends to infinity, and when $\phi = 1$, the flow is totally blocked with a permeability close to zero. This behavior reveals the potential of the model to simulate the flow through porous media with different permeability layers.

The comparison between the numerical results of the proposed model and the analytical solution shows good agreement. As inferred from Fig. 3, our model can successfully model the flow through porous media. The plotted results correspond to the first 20 lattice nodes in the y-direction beginning at the no-slip wall and extending part of the way into the bottom layer. Note that, the total number of lattices in x-direction is L_x+1 and that in y-direction is L_y+1. For the numerical values of the different simulations, please refer to Table 1.

To better understand the performance of the proposed model, further simulations are illustrated in Fig. 4 to demonstrate the behavior of the flow for different values of ϕ. Note that the model remains stable for $\tau_f \neq 1$, and we mark no changes in the performance or accuracy. The flatness in the velocity curve reveals the intensity of the resistance to the flow, which reflects its permeability conditions. By comparing the curves, we notice that the sharpness of the curve growth increases as ϕ increases. However, this increase is more relevant for low porosity, since for $\phi \geqslant 0.5$, the model reflects the flow similar to a scatter density of above 90%. This is consistent with Eq. (9).

After verifying the ability of the model to match the analytical solution, we should verify its potential to simulate the flow for different permeability layers. In the next section, we will verify the continuity of the velocity field on the interfaces of the layers.

Table 1
Table of simulation cases for the problem in Fig. 2.

	ϕ_1	ϕ_2	ϕ_3	τ_f	L_x	L_y	$L_{y1} = L_{y2} = L_{y3}$
Case 1	0.06	0.06	0.06	1	20	102	34
Case 2	0.3	0.3	0.3	1	20	102	34
Case 3	0.55	0.55	0.55	1	20	102	34
Case 4	0.2	0.2	0.2	2	20	102	34
Case 5	0.3	0.3	0.3	2	20	102	34
Case 6	0.7	0.7	0.7	2	20	102	34
Case 7	0.9	0.9	0.9	2	20	102	34
Case 8	0	0	0	1	20	102	34
Case 9	0.1	0	0.1	1	20	102	34
Case 10	0.01	0	0.01	1	20	102	34
Case 11	0.001	0	0.001	1	20	102	34
Case 12	0.2	0.1	0.2	1	20	102	34
Case 13	0.8	0.1	0.8	1	20	102	34
Case 14	0.8	0.5	0.8	1	20	102	34
Case 15	0.8	0.7	0.8	1	20	102	34
Case 16	0.5	0.4	0.6	1	20	102	34
Case 17	0.9	0.1	0.3	1	20	102	34

4. Multi-layered porous structure

4.1. Flow across multi-layers

In this section, we validate the continuity in the velocity field at the interfaces between multiple layers of differing permeability. We first recall that in the model proposed in [50], the velocity appears to be discontinuous at the interfaces, which is an unphysical behavior. Thus, an enhancement of our model will be to insure continuity at the interfaces. It is also observed that the model may not be stable when ϕ_1 and ϕ_2 are similar and closer to 1 [39]. However, this is overcome in our model. In continuum-based simulations, an interface condition coupling two different flows must be prescribed. However, because interface conditions are not uniquely defined, ambiguity rises [39]. In our model, there is no need to specify interface conditions. This ability of the model – to capture Darcy–Brinkman flow at interfaces – is the major requirement in simulating fluid flow through layered porous media. Our model is positioned to directly insure a smooth transition at the different interfaces and close to solid boundaries. This will consequently preserve continuity of the obtained macroscopic quantities.

As shown in Figs. 5 and 6, the velocity of our proposed model remains smooth when simulating different porosity layers. The simulation cases correspond to different porosity values (low and high), with various placements (low adjacent to high, high/low adjacent to high/low as listed in Table 1). The selected arrangements prove that no discontinuity is noticed; nevertheless, we note that better smoothness is associated with low porosity values (Fig. 6, Case 12).

With the presence of different porosity values adjacent to the middle layer, the behavior is affected as follows. The adjacent layer does not affect the maximum velocity. However, the effect is significant on the flatness of the curve, its sharpness, or its smoothness. This is clearly illustrated in Fig. 6b with three layers of different permeability values.

5. Analytical solutions for permeability

In this section, the simulation problem is illustrated in Fig. 7. The porosity parameter is considered constant in the first subsection; in the next sub-section an analytical solution is established to verify the model with variable porosity. It is important to verify the potential of our model to simulate a medium with any defined porosity distribution, which are commonly encountered in chemical dissolution systems [3,51].

5.1. Analytical solution for constant porosity

Another way to verify our proposed model is by comparison with the analytical solution [50] that relates the model porosity parameter to the permeability. For this purpose, the porosity

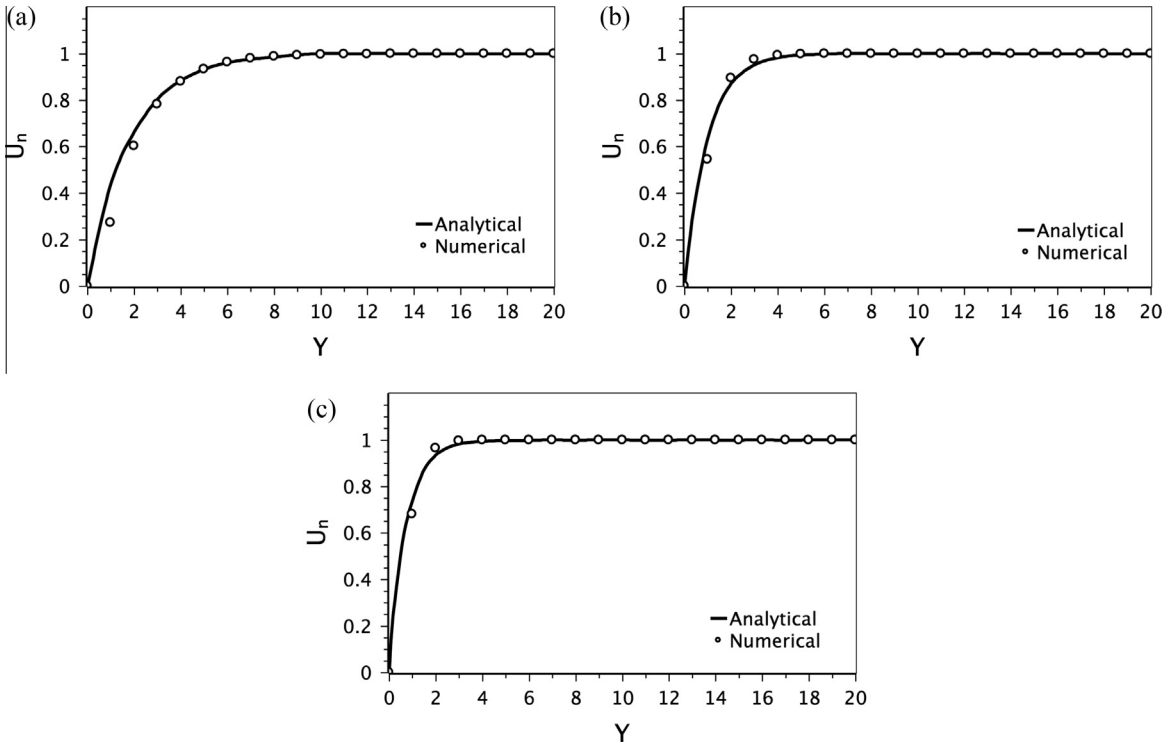

Fig. 3. Horizontal normalized velocity for the first 20 y-lattices compared to analytical solution. (a) Case 1, (b) Case 2 and (c) Case 3.

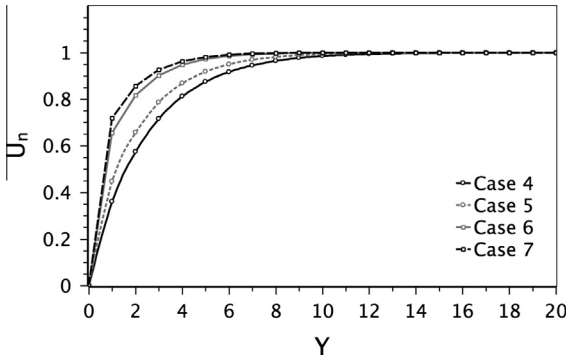

Fig. 4. Horizontal normalized velocity for different values of ϕ.

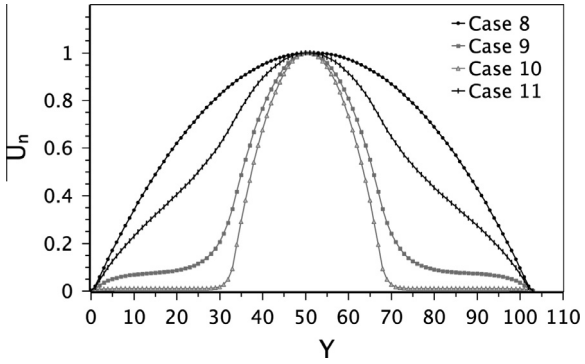

Fig. 5. Horizontal normalized velocity for multi-layers with $\phi_2 = 0$.

parameter is taken constant: $\phi(x) = \phi = constant$. However, in the following sections, we will verify the model for variable permeability and porosity.

Eq. (10) shows the analytical expression that relates the permeability, k, to the porosity parameter,

$$k = \frac{(1-\phi)v}{2\phi} \tag{10}$$

where v is the kinematic viscosity. More details on the derivation of this expression for LBM can be found in [50]. The calculation of the numerical value of k is done via Eq. (11), by applying Darcy's law [52] for a flow between two parallel plates driven by a pressure difference:

$$k = \frac{\rho v q L}{\Delta P} \tag{11}$$

where L is the length of the domain, q is the laminar fluid flux, and ΔP is the pressure difference over the length.

As shown in Fig. 8, the numerical results of the current model conform very well with the analytical solution. Hence, our method is well-verified for the calculation of Darcy flow. However, our major enhancement to the analytical relation in (Eq. (10)) will be in the implementation of an analytical solution to verify the case of having different permeability on each lattice node. This will be discussed thoroughly in the next section.

5.2. Analytical solution for variable porosity

The ability of the model to handle variable porosity is a major concern in our study. This is related to the importance of this application in natural porous media and other materials. The permeability usually varies as we go far from a solid wall or an obstacle. So practically, in our example, the permeability should vary along the y-direction, but we first verify the variable porosity model by defining a variable permeability with the channel flow

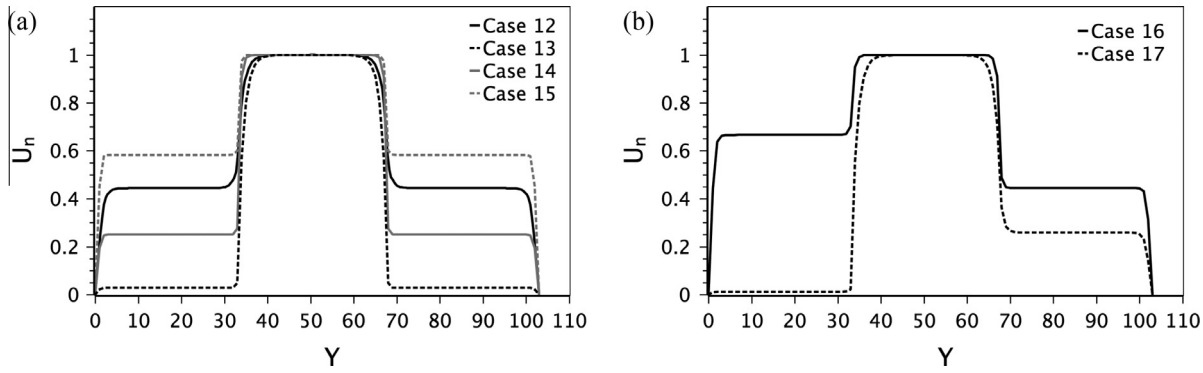

Fig. 6. Horizontal normalized velocity for multi-layers. (a) $\phi_1 = \phi_3 \neq \phi_2$ and (b) $\phi_1 \neq \phi_2 \neq \phi_3$.

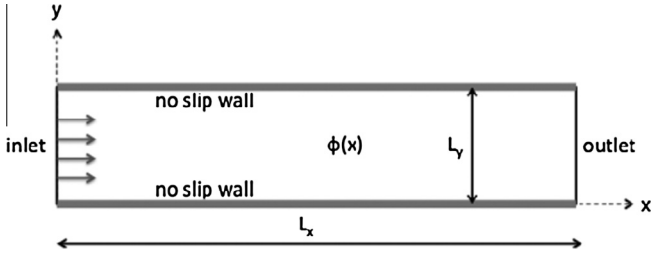

Fig. 7. Schematic view of a flow through a porous medium.

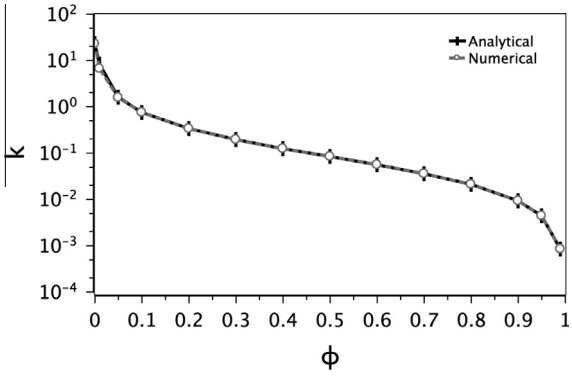

Fig. 8. Model verification: Analytical relation of permeability for constant porosity k in lattice units.

direction (along the x-direction). This is because we can derive a simple analytical solution for this case. After its validation, the model can then be applied to variable permeability across the channel.

- *Derivation of permeability relation for variable porosity along the channel.*

We will suppose that the porosity varies according to the function below:

$$\phi(x) = 0.01x = \phi_1 x \tag{12}$$

For the Lattice Boltzmann BGK model we define the following relations:

$$\begin{aligned} f_0^{eq} &= \rho\left[\tfrac{2}{3} - u^2\right] \\ f_+^{eq} &= \tfrac{\rho}{6}\left[1 + 3u + 3u^2\right] \\ f_-^{eq} &= \tfrac{\rho}{6}\left[1 - 3u + 3u^2\right] \end{aligned} \tag{13}$$

And for two adjacent nodes having the porosity as given by Eq. (12), the distribution functions are defined as:

$$\begin{aligned} f_0 &= \rho\left[\tfrac{2}{3} - u^2\right] \\ f_+^2 &= [1-\phi_1]f_+^1 + \phi_1 f_-^1 \\ f_-^1 &= [1-\phi_2]f_-^2 + \phi_2 f_+^2 \end{aligned} \tag{14}$$

In analogy with the methodology used to derive Eq. (10), we define the following parameters:

$$\begin{aligned} p &= f_+ + f_- = \rho - f_0 \\ m &= f_+ - f_- = \rho u \end{aligned} \tag{15}$$

By substitution we deduce that for two adjacent nodes 1 and 2 we have,

$$\Delta p(1,2) = 2\phi_1 m_1 + 2\phi_2 m_2 \tag{16}$$

Hence, for N nodes we have,

$$\begin{aligned} \Delta p(1,2,\ldots N) &= 2\phi_1 m_1 + 2\phi_2 m_2 + \ldots + 2\phi_N m_N \\ \Delta p(1,2,\ldots N) &= 2\phi_1\rho_1 u_1 + 2\phi_2\rho_2 u_2 + \ldots + 2\phi_N\rho_N u_N \end{aligned} \tag{17}$$

With some mathematical re-arrangements and analogy with Eqs. (8) and (11), we can derive the pressure difference as the following:

$$\begin{aligned} \Delta p &= 2\rho_0 u_0\left(\tfrac{1}{1-\phi_1}\right)[\phi_1(1-\phi_1) + \phi_1(2-2\phi_1) + \ldots + \phi_1(N - N\phi_1)] \\ \Delta p &= 2\rho_0 u_0\left(\tfrac{\phi_1}{1-\phi_1}\right)\left[N\left(\tfrac{N-1}{2}\right) - \phi_1 N\left(\tfrac{N-1}{2}\right)\right] \\ \Delta p &= 2\rho_0 u_0 N\left(\tfrac{N-1}{2}\right)\left(\tfrac{\phi_1}{1-\phi_1}\right)(1-\phi_1) \\ \Delta p &= \rho_0 u_0 \phi_1 N(N-1) = \tfrac{\rho_0 u_0 \nu N}{k} \end{aligned} \tag{18}$$

The permeability of the Nth node will be,

$$k_N = \frac{\nu}{\phi_1(N-1)} \tag{19}$$

We can define in Eq. (20) the relation between our model parameter, ϕ, and the permeability for this variable porosity medium as

$$k(x) = \frac{\nu}{\phi_1(x-1)} = \frac{\nu}{\phi(x) - \phi_1} \tag{20}$$

To verify this relation, we will solve for the pressure distribution and compare it to the numerical result. By this, we can verify that the model confirms the analytical relation for permeability (Eq. (20)).

- *Derivation of the pressure function for this problem.*

The continuity condition assures that $dq/dx = 0$. Hence, we can derive the following,

$$d[k(x)dp] = 0 \Rightarrow k(x)dp = c \Rightarrow dp = \frac{c}{k(x)} = \frac{c\phi_1(x-1)}{v} = c_1(x-1) \quad (21)$$

The analytical pressure distribution for this problem is calculated in Eq. (22),

$$p(x) = c_1\frac{x^2}{2} - c_1x + c_2 \quad (22)$$

By applying the necessary boundary conditions, we can determine the values of c_1 and c_2. The flow is driven by the pressure difference across the channel. This is, in our model, is insured by a density gradient of 0.1 mu/lu^2, with $\rho(0) = 1.1$ mu/lu^3 and $\rho(0) = 1.1$ mu/lu^3. Setting $p = \rho/3$ on boundaries, $c_1 = -6.47\times 10^{-6}$ and $c_2 = 0.3666$.

A review of Fig. 10 shows that good agreements are found between analytical and numerical pressure solutions. This proves that the relation in Eq. (20) is suitable to describe the permeability due to the variation of solid fraction satisfying Eq. (12). However, we highlight that, if we define the permeability as per Eq. (10) and derive the pressure distribution accordingly, the numerical results will be quite far from the analytical pressure.

Since the variable permeability model is well-verified, we can now use it for different applications. The function of ϕ can be now defined in any form relevant to a practical application.

6. Application to variable permeability model

In the presence of a solid boundary or multiple layers, it is often necessary to redefine the porosity and permeability near the solid wall or interface. Likewise, in some applications, such as in the design of synthetic and artificial porous media, it may be desired to have low permeability in regions near solid walls and higher permeability in regions closer to the center of the flow domain. In practice, this is insured by more compaction leading to lower porosity [53]. Ideally then, the porous medium should have a different permeability near the macroscopic boundary and the porosity reduction near the boundary may also be a continuous function. For an extensive discussion of the different features of variable permeability models, the reader can refer to the works in [53–55].

As an application, we will investigate in this section the effect of varying the permeability near the solid wall. We will define a permeability function that increases smoothly from zero on the macroscopic boundary, within a transition layer of thickness w then reaching a maximum at a central layer of constant porosity. Below, we discuss the effect of this transition layer on the velocity field and compare it to the case where this transition layer is neglected.

The flow problem in Fig. 9 is now revisited using a new function, $\phi(y)$, that varies across the channel, unlike the previous case. The function is defined as per Eq. (23), and insures a smooth passage from the transition low permeability boundary layer to the central high porosity layer with solid fraction ($\phi = 0.35$).

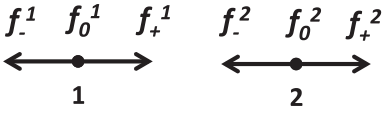

Fig. 9. Representation of the distribution functions on two adjacent nodes.

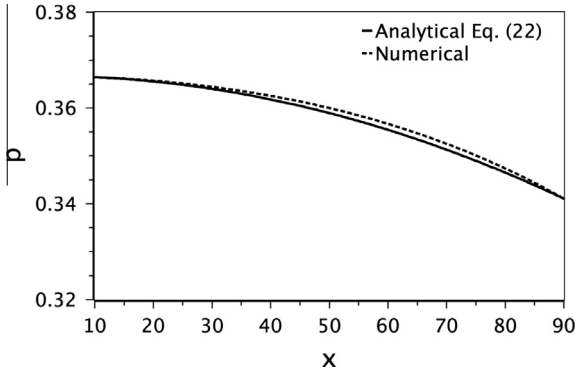

Fig. 10. Model verification: Analytical and numerical pressure distributions for variable porosity.

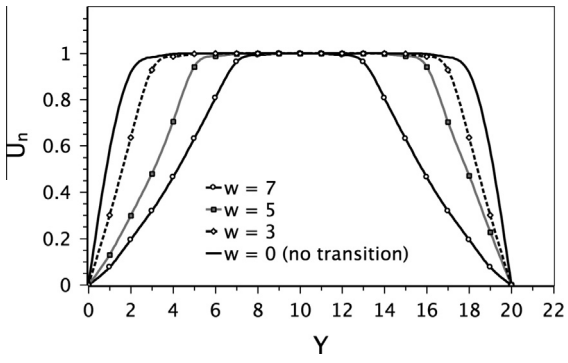

Fig. 11. Comparison of the normalized velocity in the presence and absence of a transition layer (w) with variable permeability.

$$\phi(y) = 0.007(y-w)(y-L_y+w) + 0.35 \quad (23)$$

where w denotes the thickness of the transition layer.

The effect of varying the transition layer thickness can be inferred from Fig. 11. The presence of the low permeability boundary layer increases the concavity of the velocity curve. In the absence of the transition layer the curve acquires a negative concavity, while in its presence the concavity is positive and increases with the increase of the layer's width. Hence, the behavior of the flow changes because, in the absence of any transition layer, the rate of the increase in the velocity decreases as we approach the center. However, when the layer is introduced, we assure that the rate of velocity growth increases as we approach the central layer.

The effect of the presence of the transition layer is clearly revealed in Fig. 11. As shown, even for a small width the impact on the velocity field is significant. Accordingly, we can conclude that, if this layer exists in practice, it cannot be neglected and its effect should be taken into account for a better solution of the problem.

7. Conclusion

In the present study, a new computationally efficient Gray Lattice Boltzmann model (GLBM) is developed to simulate the fluid flow in porous media. The concept of this model is close to the partial bounce-back model proposed in [50]. However, a major enhancement is in its potential to simulate the flow in variable permeability media and layers. Unlike the past model, ours shows continuity and smoothness in the velocity field at interfaces and close to solid boundaries. This is insured by defining a smooth

transition at those locations. We verified the model for the case of constant and variable porosities by comparison to analytical solutions, and permeability relations corresponding to this LBM are provided. Besides, we noted that the expression of the analytical permeability is not the same for both cases and depends on the description of the medium. The partial-bounce back adapted in this model relies on a solid fraction global parameter ϕ, which can be either constant or variable within the system. In addition, a relationship describing this parameter in terms of the actual dispersion scatter has been established. Furthermore, we underlined the importance of the potential of the model to smoothly simulate variable porosity under a wide range of applications. Sometimes, it may be desired to simulate different permeability values near solid walls and interfaces. We described the impact of creating a transition layer on the macroscopic velocity field. It is found that this layer, if present, should not be neglected in the numerical model. Taking it into consideration in the present model will clearly change the form of the velocity distribution even if its width is relatively small.

Finally, we can state that the proposed GLBM for heterogeneous permeable media has great potential, and it can be used for many different applications involving complex porous media and adjacent solids and open flow channels, so that it may enrich the research content of the emerging computational geosciences. However, to simulate heat transfer and reactive mass transport in porous media using the GLBM, there remains much to be done in the future.

References

[1] Zhao C, Hobbs BE, Ord A. Convective and advective heat transfer in geological systems. Berlin: Springer; 2008.
[2] Zhao C, Hobbs BE, Ord A. Fundamentals of computational geoscience: numerical methods and algorithms. Berlin: Springer; 2009.
[3] Zhao C. Physical and chemical dissolution front instability in porous media: theoretical analyses and computational simulations. Heidelberg: Springer; 2014.
[4] Hornby P, Ord A, Peng S, Liu L. Theoretical and numerical analyses of chemical-dissolution front instability in fluid-saturated porous rocks. Int J Numer Anal Meth Geomech 2008;32:1107–30.
[5] Zhao C, Hobbs BE, Ord A. Theoretical analyses of nonaqueous-phase-liquid dissolution induced instability in two-dimensional fluid-saturated porous media. Int J Numer Anal Meth Geomech 2010;34:1767–96.
[6] Zhao C, Hobbs BE, Ord A. Analytical solutions of nonaqueous-phase-liquid dissolution problems associated with radial flow in fluid-saturated porous media. J Hydrol 2013;494:96–106.
[7] Zhao C, Hobbs BE, Ord A. Effects of domain shapes on the morphological evolution of nonaqueous-phase-liquid dissolution fronts in fluid-saturated porous media. J Contam Hydrol 2012;138–139:123–40.
[8] Hobbs BE, Ord A, Peng S. Effects of mineral dissolution ratios on chemical-dissolution front instability in fluid-saturated porous media. Transp Porous Media 2010;82:317–35.
[9] Ord A, Hornby P, Peng S. Effect of reactive surface areas associated with different particle shapes on chemical-dissolution front instability in fluid-saturated porous rocks. Transp Porous Media 2008;73:75–94.
[10] Zhao C, Hobbs BE, Ord A. Theoretical analyses of acidization-dissolution front instability in fluid-saturated carbonate rocks. Int J Numer Anal Meth Geomech 2013;37:2084–105.
[11] Poulet T, Regenauer-Lieb K, Hobbs BE. Computational modeling of moving interfaces between fluid and porous medium domains. Comput. Geosci. 2013;17:151–66.
[12] White JA, Borja RI, Fredrich JT. Calculating the effective permeability of sandstone with multiscale Lattice Boltzmann/finite element simulations. Acta Geotech 2006;1:195–209.
[13] Bear J, Corapcioglu MY. Advances in transport phenomena in porous media. Springer; 1987.
[14] Bachmat Y, Bear J. On the concept and size of a representative elementary volume (Rev). Advances in transport phenomena in porous media. NATO ASI Ser 1987;128:3–20.
[15] Costanza-Robinson MS, Estabrook BD, Fouhey DF. Representative elementary volume estimation for porosity, moisture saturation, and air-water interfacial areas in unsaturated porous media: data quality implications. Water Resour Res 2011;47:07513.
[16] Ord A, Hornby P, Peng S. Morphological evolution of three-dimensional chemical dissolution front in fluid-saturated porous media: a numerical simulation approach. Geofluids 2008;8:113–27.
[17] Hornby P, Peng S, Liu L. Mineral precipitation associated with vertical fault zones: the interaction of solute advection, diffusion and chemical kinetics. Geofluids 2007;7:3–18.
[18] Reid LB, Regenauer-Lieb K. Some fundamental issues in computational hydrodynamics of mineralization: a review. J Geochem Explor 2012;112:21–34.
[19] Zhao C, Hobbs BE, Ord A. Theoretical analyses of the effects of solute dispersion on chemical-dissolution front instability in fluid-saturated porous rocks. Transp Porous Media 2010;84:629–53.
[20] Zhao C, Hobbs BE, Ord A. Effects of medium and pore-fluid compressibility on chemical-dissolution front instability in fluid-saturated porous media. Int J Num Analy Meth Geomech 2012;36:1077–100.
[21] Reid LB, Regenauer-Lieb K, Poulet T. A porosity-gradient replacement approach for computational simulation of chemical-dissolution front propagation in fluid-saturated porous media including pore-fluid compressibility. Comput Geosci 2012;16:735–55.
[22] Hobbs BE, Ord A. Effects of medium permeability anisotropy on chemical-dissolution front instability in fluid-saturated porous rocks. Transp Porous Media 2013;99:119–43.
[23] Peng S, Mühlhaus HB, Liu L. Theoretical investigation of convective instability in inclined and fluid-saturated three-dimensional fault zones. Tectonophysics 2004;387:47–64.
[24] Zhao C, Hobbs BE, Ord A. Investigating dynamic mechanisms of geological phenomena using methodology of computational geosciences: an example of equal-distant mineralization in a fault. Sci China, Ser D Earth Sci 2008;51:947–54.
[25] Ord A, Peng S, Liu L. Inversely-mapped analytical solutions for flow patterns around and within inclined elliptic inclusions in fluid-saturated rocks. Math Geosci 2008;40:179–97.
[26] Poulet T, Regenauer-Lieb K. Numerical modeling of toxic nonaqueous-phase-liquid removal from contaminated groundwater systems: mesh effect and discretization error estimation. Int J Num Analy Meth Geomech 2015;39:571–93.
[27] Poulet T, Regenauer-Lieb K. Replacement of annular domain with trapezoidal domain in computational modeling of nonaqueous-phase-liquid dissolution-front propagation problems. J Central South Univ 2015;22:1841–6.
[28] Zhao C. Advances in numerical algorithms and methods in computational geosciences with modeling characteristics of multiple physical and chemical processes. Sci China Ser E: Technol Sci 2015;58:783–95.
[29] Hobbs BE, Ord A. Theoretical analyses of chemical dissolution-front instability in fluid-saturated porous media under non-isothermal conditions. Int J Num Analy Meth Geomech 2015;39:799–820.
[30] Hobbs BE, Ord A. Computational simulation of chemical dissolution-front instability in fluid-saturated porous media under non-isothermal conditions. Int J Num Meth Eng 2015;102:135–56.
[31] Hobbs BE, Ord A. Particle simulation of spontaneous crack generation associated with the laccolithic type of magma intrusion processes. Int J Num Meth Eng 2008;2008(75):1172–93.
[32] Sukop MC, Thorne DT. Lattice boltzmann modeling: an introduction for geoscientists and engineers. Berlin: Springer; 2006.
[33] Bouzidi M, d'Humières D, Lallemand P, Luo LS. Lattice Boltzmann equation on a two-dimensional rectangular grid. J Comput Phys 2001;172:704–17.
[34] Succi S. The Lattice Boltzmann equation for fluid dynamics and beyond. Oxford: Oxford Univ Press; 2001.
[35] Chen S, Doolen GD. Lattice Boltzmann method for fluid flows. Annu Rev Fluid Mech 1998;30:329–64.
[36] Rothman D. Cellular-automaton fluids: a model for flow in porous media. Geophysics 1988;53(4):509.
[37] Succi S, Foti E, Higuera F. Three-dimensional flows in complex geometries with the Lattice Boltzmann method. Europhys 1989;10(5):433. Letters.
[38] Quan L, Tien-Chien J. Application of Lattice Boltzmann method in fluid flow and heat transfer. InTech 2011:29–32. ISBN 978-953-307-169-5.
[39] Jiujiang Z, Jingsheng M. An improved gray lattice Boltzmann model for simulating fluid flow in multi-scale porous media. Adv Water Resour 2013;56:61–76.
[40] Guo ZL, Zhao TS. Lattice Boltzmann model for incompressible flows through porous media. Phys Rev E 2002:66.
[41] Freed DM. Lattice-Boltzmann method for macroscopic porous media modeling. Int J Mod Phys C 1998;9:1491–503.
[42] Kang QJ, Zhang DX, Chen SY. Unified lattice Boltzmann method for flow in multiscale porous media. Phys Rev E 2002:66.
[43] Spaid MAA, Frederick J, Phelan R. Lattice Boltzmann methods for modeling microscale flow in fibrous porous media. Phys Fluids 1997;9:2468–74.
[44] Anwar S, Sukop MC. Lattice Boltzmann models for flow and transport in saturated karst. Ground Water 2009;47:401–13.
[45] Chen C, Packman AI, Gaillard JF. Pore-scale analysis of permeability reduction resulting from colloid deposition. Geophys Res Lett 2008:35.
[46] Nie XB, Martys NS. Breakdown of Chapman–Enskog expansion and the anisotropic effect for lattice-Boltzmann models of porous flow. Phys Fluids 2007:19.
[47] Dardis O, McCloskey J. Lattice Boltzmann scheme with real numbered solid density for the simulation of flow in porous media. Phys Rev E 1998;57 (4):4834–7.
[48] Dardis O, McCloskey J. Permeability porosity relationships from numerical simulations of fluid flow. Geophys Res Lett 1998;25:1471–4.

[49] Thorne D, Sukop MC. Lattice Boltzmann model for the Elder problem. In: Proceedings of the XVth international conference on computational methods in water resources (CMWR XV), Chapel Hill, NC, USA, June 13–17. Amsterdam: Elsevier; 2004. p. 1549–1557.
[50] Walsh SDC, Burwinkle H, Saar MO. A new partial-bounceback lattice-Boltzmann method for fluid flow through heterogeneous media. Comput Geosci 2009;35:1186–93.
[51] Zhao C, Hobbs BE, Ord A. Theoretical and numerical investigation into roles of geofluid flow in ore forming systems: Integrated mass conservation and generic model approach. J Geochem Explor 2010;106:251–60.
[52] Darcy H. Les Fontaines Publiques de la Ville de Dijon (The Public Fountains of the City of Dijon). Paris: Dalmont; 1856.
[53] Hamdan MH, Kamel MT. Flow through variable permeability porous layers. Adv Theor Appl Mech 2011;4(3):135–45.
[54] Rees DAS, Pop I. Vertical free convection in a porous medium with variable permeability effects. Int J Heat Mass Transf 2000;43:2565–71.
[55] Sahraoui M, Kaviany M. Slip and no-slip velocity boundary conditions at interface of porous plain media. Int J Heat Mass Transfer 1992;35:927–43.